Synthesis of butyl-exchanged polyoxymethylene ethers as renewable diesel blendstocks with improved fuel properties

Martha A. Arellano-Treviño,[a] Danielle Bartholet,[b] Anh The To,[a] Andrew W. Bartling,[a] Frederick G. Baddour,[a] Teresa L. Alleman,[c] Earl D. Christensen,[a] Gina M. Fioroni,[c] Cameron Hays,[c] Jon Luecke,[c] Junqing Zhu,[d] Charles S. McEnally,[d] Lisa D. Pfefferle,[d] Kenneth F. Reardon,[b] Thomas D. Foust,[a] Daniel A. Ruddy[a]**

[a]Catalytic Carbon Transformation & Scale-up Center, National Renewable Energy Laboratory, Golden, Colorado 80401, USA.

[b]Department of Chemical and Biological Engineering, Colorado State University, Fort Collins, Colorado 80523, United States.

[c]Center for Integrated Mobility Sciences, National Renewable Energy Laboratory, Golden, Colorado 80401, United States.

[d]Department of Chemical and Environmental Engineering, Yale University, New Haven, Connecticut 06520, United States.

Abstract

Methyl-terminated polyoxymethylene ethers (MM-POMEs), having the formula CH_3O-$(CH_2O)_n$-CH_3 (n = 3-5), are a high-cetane, low-sooting group of oxygenates that have recently attracted attention as potential diesel blendstocks. Despite these attractive fuel properties, MM-POMEs have shortcomings due to their low energy density and high water solubility. Guided by a computational fuel property assessment for POMEs with longer end-groups, the most promising improvements in the desired compression ignition fuel properties were observed for butyl-terminated POMEs. Here, an acid-catalyzed trans-acetalization reaction was developed to exchange the methyl end-groups of MM-POMEs (n = 3-6) with butyl end-groups. The reaction utilizes an ion-exchange resin as the acid catalyst at mild reaction conditions of 60 °C and atmospheric pressure. Approximately 100 mL of butyl-exchanged POMEs in the diesel boiling range were produced, enabling laboratory-scale fuel property testing. The butyl-terminated POME mixture possesses the advantaged fuel properties of the parent MM-POMEs (low-soot, high-cetane) while exhibiting improved energy density (Lower Heating Value (LHV) of 30 MJ/kg) and substantially reduced water solubility (7.3 g/L) compared to the parent MM-POME mixture (LHV of 19 MJ/kg , water solubility of 258 g/L).

KEYWORDS. Bio-derived blendstocks, polyoxymethylene ethers, trans-acetalization, water solubility, lower heating value

Introduction

Heavy-duty truck vehicle miles traveled in the U.S., which rely on diesel-fueled compression ignition (CI) engines, are expected to increase 38% by 2050.[1] Despite the projected increase in miles traveled, it is also expected that the energy intensity (i.e., energy per ton-mile traveled) will decrease, attributed to vehicle efficiency standards taking full effect.[1,2] Enhanced fuel properties play a major role in the improvement of fuel economy and engine efficiency. Simultaneously, low-net-carbon and low-emission (e.g., soot, NOx) fuels are required to meet the fuel demand in an environmentally conscious and sustainable way. Methyl-terminated polyoxymethylene ethers (MM-POMEs) having the chemical formula, $CH_3O\text{-}(CH_2O\text{-})_n\text{-}CH_3$ (n = 3-5) are a class of low-soot, high-cetane oxygenates that have recently received attention as CI or diesel fuel blendstocks.[3–7] Methanol (MeOH) and its derivative, formaldehyde, are the primary chemicals utilized for MM-POME synthesis,[8] and therefore, a low carbon-intensity POME-based fuel can be derived from ligno-cellulosic biomass via biomass gasification and methanol synthesis.[9–15]

As a proof of concept, our research group recently reported a one-step synthesis of dimethoxymethane (DMM), the simplest POME, from MeOH.[16] Despite the advantage of a low Yield Sooting Index (YSI), DMM by itself would not be an acceptable CI fuel, having unacceptably low values for cetane number (CN), lower heating value (LHV), flash point (T_{flash}), boiling point (T_b), and a high water solubility.[17] Rather, a mixture of MM-POMEs with medium chain lengths of 3-5 (termed here MM-$POME_{3\text{-}5}$), possesses more suitable CI fuel properties.[7,18–22] However, there is a significant concern about the limited fuel efficiency due to their low energy density (LHV). In addition, the high water solubility of MM-POMEs hinders their large-scale deployment on different fronts, such as difficulty in keeping the blendstock dry during distribution and risks of water source contamination upon leakage from any part of the fueling infrastructure.

A set of blendstock screening criteria, termed Tier 1, has been defined based on previously reported fuel characteristics for CI fuels (Table 1). The ASTM specification for diesel fuel (ASTM D975-20a)[23,24] stipulates a diesel boiling range between 180 – 338 °C; however, Tier 1 extends the boiling range to 160 – 338 °C where the floor value is dictated by the upper limit requirements of the fuel blendstocks for advanced spark-ignition (gasoline) engines[25] and the ceiling represents the diesel T90 upper limit dictated by the ASTM specification. The limit for cloud point (T_{cloud}) is less than 0 °C, to ensure operability at low temperatures in engines and along the fueling infrastructure.[24] The Tier 1 criteria specify that the essential safety property of flash point is greater than 52 °C to ensure safe handling at normal atmospheric conditions as stipulated by ASTM D975-20a.[23,24] CN values of at least 40 are required to ensure ignition quality and meet the ASTM D975-20a specification.[23,24] YSI values, a measure of the tendency of a fuel to form soot when combusted,[26] are targeted to be below the value for a certification diesel fuel of 246.[27] A greater LHV results in improved fuel economy, and the Tier 1 criterion stipulates at least 25 MJ/kg, which is comparable to the LHV reported for ethanol (26.8 MJ/kg). This criterion ensures that the LHV penalty of a new diesel blendstock will be comparable to that of E10 gasoline.[28] Finally, the water solubility criterion is less than 20 g/L to prevent phase separation in the distribution system and minimize potential groundwater contamination.[24]

Table 1. Tier 1 criteria for compression ignition (CI) fuel properties.[23-25, 27, 28]

Fuel Property	Criteria Limit
Boiling point (°C)	160 – 338
Cloud Point (°C)	< 0
Flash point (°C)	> 52
Cetane number	≥ 40
YSI	< 246
LHV (MJ/kg)	> 25
Water solub. (g/L)	< 20

The development of bio-derived CI fuels can benefit from a fuel-property-first approach, a method that has been successfully implemented to identify and produce diesel blendstocks from bio-derived carboxylic acids.[29–31] In addition to chain length noted above, the alkyl-terminating group also affects the fuel properties of POMEs. A recent report prepared ethyl-terminated POMEs, which exhibited greater heating values and lower autoignition points compared to their methyl-terminated counterparts.[19] These results informed our hypothesis that end-group exchange with larger alcohols, such as 1-propanol and 1-butanol (BuOH), could further benefit the fuel properties, especially decreasing the water solubility due to the incorporation of larger hydrophobic moieties. Importantly, these alcohols have the potential to be renewably sourced, especially ethanol and BuOH.[32,33] In a related report, computational tools were utilized to predict the Tier 1 fuel properties of the newly targeted propyl- and butyl-terminated POME structures.[27] The structures are termed

MM-, EE-, PP-, and BB-POME$_n$ where MM, EE, PP and BB denote the two methyl, ethyl, propyl and butyl end-groups, respectively, and n is the chain length. The results were compared to the Tier 1 criteria and previously reported values of MM- and EE-POMEs, enabling trends to be identified across chain length (n = 1-4) and end-group. The properties of LHV and water solubility were problematic for the parent MM-POME$_n$ structures, and a clearly visible advantage can be observed in the calculated improvements when incorporating longer alkyl end-groups (Figure 1). Specifically, BB-POME$_{1\text{-}4}$ possess the most desirable properties, especially considering the critical water solubility metric, motivating the development of chemistry to upgrade a MM-POME$_n$ mixture into a product having enhanced fuel properties.

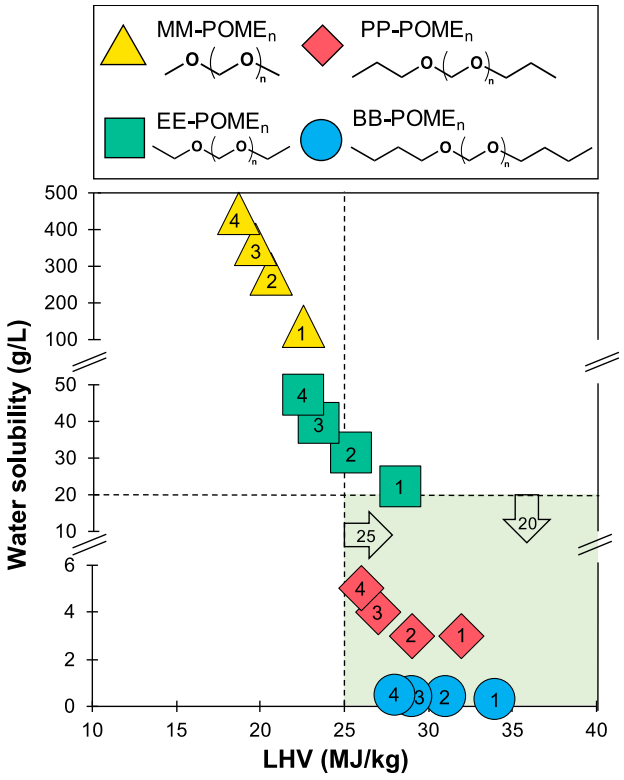

Figure 1. Predicted and measured water solubility (g/L) and LHV (MJ/kg) of ethyl (EE), propyl (PP) and butyl (BB) exchanged MM-POME$_n$ (n = 1- 4). Diesel blendstock fuel property criteria limits are represented by dotted lines and target area is highlighted in light green. Chain lengths (n

= 1-4) within the same end-group are represented by the increased numeration within the same marker type. Values are tabulated in Table S1 including predicted values from Bartholet, et al.[27]

There are several synthetic strategies for the production of POMEs reported in the literature, and most of them incorporate formaldehyde as a reactant.[6,7,19,34] Here we report a conversion pathway to generate the computationally-identified BB-POME$_n$ species through the reaction of a parent MM-POME$_{3-6}$ mixture with BuOH. This choice of reactants has the advantage of avoiding the use of formaldehyde in the transacetalization chemistry and the associated carbon loss and drying cost for anhydrous formaldehyde production, which is critical for sustainable and economical production of POMEs.[16] The targeted product was synthesized under relatively mild conditions in a scalable reactor and separated in the desired boiling range by spinning band distillation. The fuel properties of the butyl-terminated product were measured experimentally following ASTM standards and compared against their predicted values, the measured values of the parent MM-POME$_n$ mixture, and the CI Tier 1 criteria in Table 1.

Results and Discussion

Catalytic end-group exchange. For the end-group exchange chemistry, a trans-acetalization reaction was investigated at 60 °C using an acidic Amberlyst-46 catalyst (4.6 wt% with respect to the total mass of reactants), which is from the same family of sulfonic acid resins that perform similar transformations of alcohols with cyclic ethers at similar temperatures (Scheme 1).[6,7,20,35–38] Crude products were analyzed using gas chromatography (Figure S1) and ^{13}C NMR spectroscopy. The thermodynamic limit for the trans-acetalization reaction was calculated assuming system ideality to enable a comparison of experimentally observed product selectivity

for both end-group exchange and chain length. Detailed Aspen Plus calculation results are presented in Figure S2 and Table S2. Control experiments of the parent MM-POME$_{3\text{-}6}$ mixture and BuOH without the acid catalyst, or in the presence of catalyst but without BuOH, exhibited no exchange of the methyl end-groups of the parent MM-POMEs (Figure S3 and Table S3).

Scheme 1. The acid-catalyzed trans-acetalization reaction of BuOH with MM-POME$_{3\text{-}6}$. B and M represent butyl and methyl groups, respectively.

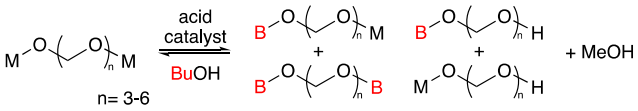

The product distribution of the trans-acetalization reaction with 2:1 BuOH:MM-POME$_{3\text{-}6}$ was followed over 24 h. This initial assessment of the chemistry focused on quantification of the acetal products, and hemiacetal products were not explicitly quantified (*vide infra*). Figure 2 presents the relative product distribution of the 7 most abundant components observed at 1, 2, 4, 6 and 24 h. Under these conditions, the reaction proceeded rapidly, indicated by the fast BuOH consumption and formation of MB-POME$_n$ (i.e., single exchange giving methyl-butyl end-groups) and BB-POME$_n$ after 1 h. The relative product distribution exhibited only minor changes from 4 h to 24 h, indicative of reaching equilibrium. Therefore, 4 h was chosen as a suitable reaction time for comparison in subsequent reactions.

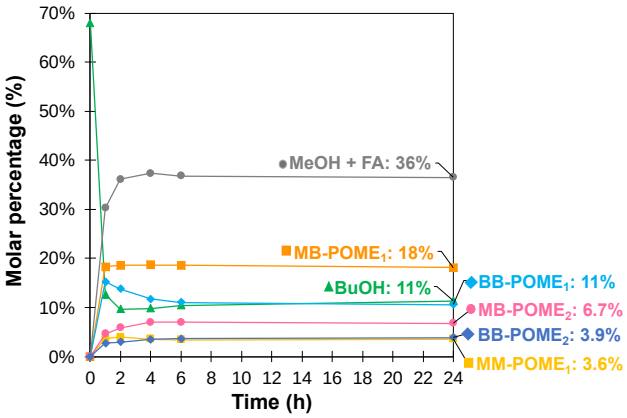

Figure 2. Relative product distribution of the 7 most abundant compounds during catalytic end-group exchange with 2:1 BuOH:MM-POME$_{3\text{-}6}$ molar ratio over 24 h of reaction at 60 °C and atmospheric pressure using 4.6 wt% of Amberlyst-46 catalyst. Relative distribution of GC-observed species is presented in Table S4.

Figure 3A presents the relative acetal product distribution from the trans-acetalization reaction with varying molar ratios of BuOH:MM-POME$_{3\text{-}6}$ at 60 °C and atmospheric pressure over 4.6 wt% of Amberlyst-46 for 4 h. With a stoichiometric molar ratio of 2:1, substantial butyl exchange was observed, yielding 47 wt% of the single-exchanged and 41 wt% double-exchanged products. These results demonstrated a simple route to incorporate higher alcohols into the POME structures under mild reaction conditions. It is also important to note that the acidic ion-exchange resin Amberlyst-46 catalyst is required for the end-group exchange reaction, and the reaction did not occur at the studied conditions without catalyst (Figure S3, Table S3). Reactions with excess BuOH were investigated with two additional molar ratios of 4:1 and 10:1 for BuOH:MM-POME$_{3\text{-}6}$. With excess BuOH, dibutyl-exchange to yield BB-POME$_n$ increased with a concomitant decrease in single-exchanged MB products, with the 4:1 ratio yielding 58 wt% BB products and the 10:1 ratio yielding 73 wt% BB products. These results are in agreement with the predicted thermodynamic

limitations of the exchange chemistry that indicate increased exchange of MM-POME$_n$ end-groups with increasing initial ratios of BuOH:MM-POME$_{3\text{-}6}$ (Figure S2, Table S2). A portion of the MM-POME$_{3\text{-}6}$ starting material remained even when excess alcohol was used (12 wt%, 6 wt% and 5 wt% for the 2:1, 4:1 and 10:1 ratio respectively, Figure 3A), in line with the thermodynamic limitations (Figure S2).

During the end-group exchange reaction, the chain lengths redistributed to a range of n = 1-6, with n=1 being most abundant at 60 wt% for the 2:1 ratio (Figure 3B), 86 wt% for the 4:1 ratio and up to 97 wt% for the 10:1 ratio. As a reference, the composition of the parent MM-POME$_{3\text{-}6}$ is 45.6 wt% MM-POME$_3$, 30.4 wt% MM-POME$_4$, 17.8 wt% MM-POME$_5$, and 6.1 wt% MM-POME$_6$. Thermodynamic calculations for the trans-acetalization reaction indicate that the breakdown of longer MM-POMEs with n = 3-6 into shorter chains with n = 1-2 is energetically favored (K_{eq} = 102, Rxn# 15-18, 20-24 in Table S5). As outlined by the computational analysis, the BB end-groups offset the detrimental effect of chain shortening by shifting the fuel properties of n = 1-2 POMEs into the desired, advantageous range. The control experiment without BuOH demonstrated that the parent POMEs undergo a redistribution of chain lengths with Amberlyst-46, giving a distribution in the range of n = 1-8 with n = 3 being most abundant at 33 wt% (Figure S3). The control experiment without catalyst confirmed that no end-group exchange chemistry occurred in the absence of catalyst, and further, the chain lengths were not redistributed.

Our analysis of the products from varying molar ratios of BuOH:MM-POME$_{3\text{-}6}$ focused on the acetal products, however, hemiacetal (HA) products also form in this reaction, as noted in Scheme 1 and the thermodynamic calculations (Table S5). HA products have been reported to decompose

during the GC analysis to formaldehyde, methanol and/or butanol,[39,40] all of which can be quantified using GC analysis. However, formaldehyde is notoriously difficult to quantify using GC and could lead to error in the analysis. For the reaction with a 2:1 molar ratio of BuOH:MM-POME$_{3\text{-}6}$, the carbon balance for products observed using the GC method was determined to be 91%. For reactions with molar ratios of 4:1 and 10:1, the carbon balances were ≥98%. This comparatively low carbon balance from the reaction with a 2:1 molar ratio, where one would expect a greater HA concentration due to the lower butanol concentration, highlights the difficulty in quantifying hemiacetals and formaldehyde by GC. Even with a high carbon balance, as observed for the products from 4:1 and 10:1 molar ratios, the method remains blind to HA species. As an alternative analysis method, ^{13}C NMR spectroscopy allows for direct observation of HAs.[39] The ^{13}C NMR spectra exhibited a complex peak pattern due to the mixture of species having methyl and butyl termination, but three unique resonances could be assigned to the presence of three expected hemiacetals based on previous reports of similar species:[18,41,42] B-POME$_1$-HA (BuO-**C**H$_2$-OH) at δ 89.9 for the bolded C, M-POME$_1$-HA (MeO-**C**H$_2$-OH) at δ 91.0, and B-POME$_2$-HA (BuO-**C**H$_2$O-CH$_2$-OH) at δ 91.8 (Figure S4). Integration of these peaks relative to the concentration of BB-POME$_1$ (δ 95.8) determined from GC analysis enabled an estimation of the HA content in the crude products from each reaction. The crude products from the reactions with 2:1 and 4:1 molar ratios had 17.5 mol% HA, and the crude product from the reaction with a 10:1 molar ratio had 4.2 mol% HA. This lower HA concentration from the reaction with a high BuOH:MM-POME$_{3\text{-}6}$ ratio of 10:1 is in agreement with the thermodynamic calculations. Similarly, although the same total HA content of 17.5 mol% was found for the products from the 2:1 and 4:1 reactions, the ratio of B-POME$_1$-HA to M-POME$_1$-HA increased from 0.90 to 2.1 mol/mol when the BuOH:MM-POME$_{3\text{-}6}$ ratio increased. HA products were indirectly quantified

in the GC analysis as methanol, butanol, and formaldehyde, but this ^{13}C NMR spectroscopic analysis provided a direct assessment of their structure and content in the crude products.

The crude product mixture of butyl-terminated POMEs contains undesirable light components, such as water, HAs, MeOH and unreacted BuOH, that lie outside of the desired boiling point range (160 – 338 °C). The relative portion of the crude product that lies within the desired boiling point range is presented in Figure 3C in two groups: all combinations of end-groups in the target T_b range (i.e., MM + MB + BB), and only the butyl-terminated (MB + BB) species. The reaction with a 2:1 BuOH:MM-POME$_{3\text{-}6}$ ratio yielded 50 wt% of the products in the desired boiling point range with 49 wt% corresponding to butyl-terminated POMEs. With an initial BuOH:MM-POME$_{3\text{-}6}$ ratio of 4:1, a comparable portion of the product distribution was in the desired boiling point range (54 wt%), with 52 wt% corresponding to butyl-terminated POMEs. Increasing the initial BuOH:MM-POME$_{3\text{-}6}$ ratio to 10:1 promoted the double end-group exchange reaction; however, the excess BuOH diluted the composition, resulting in a lower fraction of the crude product mixture in the desired boiling point range (41 wt%). Finally, it is worth noting that for the 2:1 and 4:1 molar ratios, 97-98 wt% of the products in the desired boiling point range corresponded to butyl-terminated POMEs, which are the target products with enhanced fuel properties identified from the computational analysis. The 2:1 molar ratio was chosen to prepare a large batch of butyl-exchanged product, due to the combination of an adequate end-group exchange yield in the desired distillate boiling range (49 wt%) and the minimum volume of BuOH to be separated from the product.

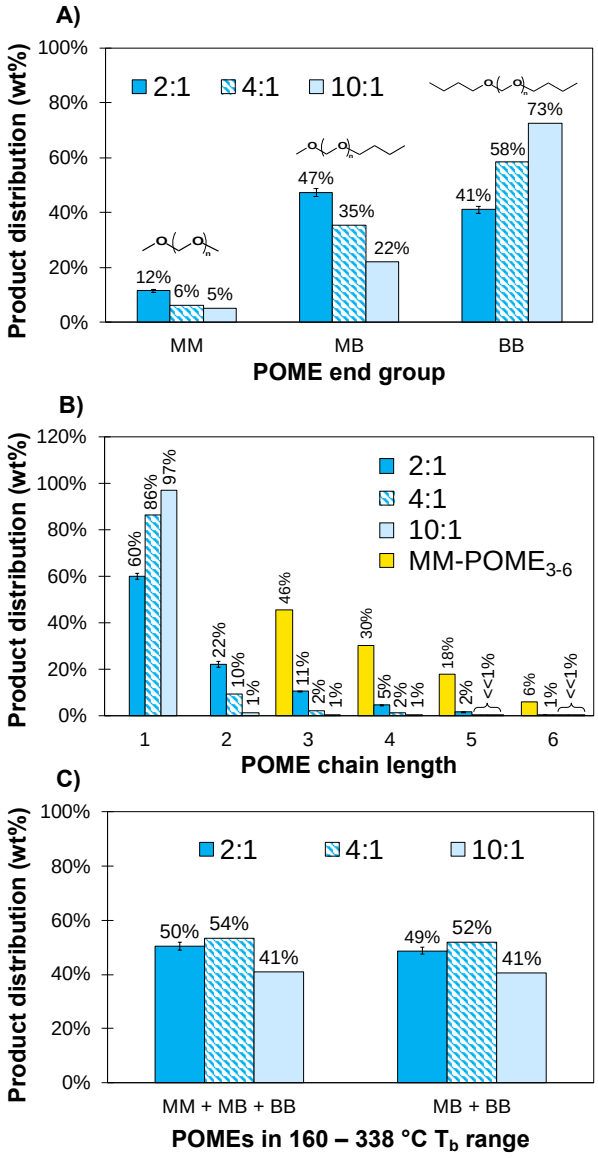

Figure 3. Relative product distribution of A) exchanged end-groups, B) POME chain length and C) fraction of product in the desired boiling point range after catalytic end-group exchange reactions with 2:1, 4:1, and 10:1 BuOH:MM-POME$_{3\text{-}6}$ molar ratios. Chain length distribution for the parent MM-POME$_{3\text{-}6}$ is included in B) for reference. Detailed relative product distributions reported in Table S6. Standard error bars included for the 2:1 BuOH:MM-POME$_{3\text{-}6}$ molar ratio condition based on results from triplicate experiments (Table S7).

Separation of desired products. Distillation of the butyl-terminated POME product mixture was performed, targeting a product in the boiling point range of 160 – 338 °C. To reduce the presence of reactive light species in the product (e.g., residual formaldehyde, HAs, water, MeOH, DMM, BuOH) during distillation, the crude product was washed with a carbonate-buffered aqueous solution (pH = 9.2) followed by a vacuum treatment at 50 °C and 50 mbar. This treatment of the butyl-terminated POME product resulted in a decrease of light species from 21 wt% to 5 wt% of total mass (Table S8). The washed product was readily separated in a spinning band distillation column to yield approximately 100 mL of the targeted MB- and BB-terminated POME product in the 160 – 338 °C boiling point range. This distilled product is referred to as B*POME$_{1\text{-}6}$. As presented in Table 2, 46 wt% of B*POME$_{1\text{-}6}$ corresponded to the major product from the reaction, BB-POME$_1$ (i.e., butylal). This individual compound has already been investigated as a promising diesel blendstock, and has passed Tier 1 criteria.[24] Notably, the HA content in this distilled product was negligible, evidenced by the butylal analysis of B*POME$_{1\text{-}6}$ fitting the GC calibration curve (Figure S1) and the absence of resonances corresponding to HA species in the ^{13}C NMR spectrum (Figure S4).

Table 2. Water-free product composition of B*POME$_{1-6}$. Water content was 0.42 wt% as measured by Karl-Fischer titration.

ID	Desired product T_b 160 – 338 °C (B*POME$_{1-6}$)	
	mol%	wt%
BuOH	0.1	< 0.1
BB-POME$_1$	48	46
MM-POME$_2$	0.1	0.1
MB-POME$_2$	17	14
BB-POME$_2$	14	16
MM-POME$_3$	0.1	0.1
MB-POME$_3$	8.6	8.6
BB-POME$_3$	4.2	5.4
MM-POME$_4$	1.2	0.8
MB-POME$_4$	3.3	3.9
BB-POME$_4$	1.2	1.7
MM-POME$_5$	0.8	0.9
MB-POME$_5$	0.7	1.0
BB-POME$_5$	0.5	0.8
MM-POME$_6$	0.2	0.3
MB-POME$_6$	0.2	0.3

Measured fuel properties. The fuel properties of B*POME$_{1-6}$ were measured experimentally and compared to their predicted fuel properties (Figure 4). The predicted values were calculated assuming a linear blending of its individual components using the appropriate units for each property (i.e., mol% for CN and YSI; wt% for LHV and water solubility; and vol% for T_b, T_{cloud}, and T_{flash}). The measured properties of B*POME$_{1-6}$ were compared to the Tier 1 criteria and the measured fuel properties of MM-POME$_{3-6}$, BB-POME$_1$, and EE-POME$_3$. All of these POMEs are good reference points to the B*POME$_{1-6}$ product since they encompass a variety of end-groups and chain lengths for comparison of fuel property values.

The B*POME$_{1-6}$ product lies in the target boiling range with a measured T10 and final boiling point of 169 – 287 °C (Table S9). The parent POMEs have a measured boiling range of 156 – 259 °C,[21] where the lower limit is slightly out of the target (160 – 338 °C). Both BB-POME$_1$ and EE-POME$_3$ are pure components with boiling points of 179 °C and 185 °C, respectively. All compared POMEs exceeded the T_m (for pure components) or T_{cloud} (for mixtures) value requirement of < 0 °C. The cloud point of the B*POME$_{1-6}$ was calculated by assuming a linear blending of the predicted melting points (T_m) of the pure components in the product. The measured cloud point was -27 °C, overpredicted by 4 °C. This error is common for melting point calculations; with publications reporting root-mean-square errors up to 52 °C.[43] The T_{flash} values were comparable among MM-POME$_{3-6}$ (63 °C), BB-POME$_1$ (62 °C), and B*POME$_{1-6}$ (62 °C, overpredicted by 7 °C), with a slightly higher value for EE-POME$_3$ (68 °C), all meeting the required criterion of >52 °C.

The measured cetane number of the B*POME$_{1-6}$ was 75, almost double the minimum requirement (> 40). This high cetane value is in a similar range to the comparative POMEs, being slightly greater than the MM-POME$_{3-6}$ (CN=73) and BB-POME$_1$ (70), but slightly lower than EE-POME$_3$ (CN=80). The measured YSI of 37 for B*POME$_{1-6}$ was accurately predicted and is greater than the extremely low value of the MM-POME$_{3-6}$ (YSI=2.1), which is attributed to the absence of C-C bonds in their molecular structure. Considering the mix of methyl and butyl moieties in B*POME$_{1-6}$, the YSI value of 37 between EE-POME$_3$ (predicted YSI=26) and BB-POME$_1$ (YSI=48) follows the same C-C bond reasoning. Despite the increase in YSI for B*POME$_{1-6}$ compared to the starting MM-POME$_{3-6}$, the value lies well below that of a representative

certification diesel fuel (< 246)[27], retaining the advantaged low-sooting properties of POMEs. CN was overpredicted by 17.3%. Computational models for predicting cetane number have been reported with typical errors of +/- 10 CNs, and we associate the high relative error observed for the butyl-terminated product to the unique molecular structure of these POMEs not being adequately represented in the training data set used to develop the prediction models.[44–46] The measured LHV of 30 MJ/kg for B*POME$_{1\text{-}6}$ was in accordance with the predicted linear blending estimate (3.3% error) and exceeded the minimum requirement for this criterion (>25 MJ/kg). This value represents an important improvement to this critical fuel property over the low LHV values of the parent MM-POME$_{3\text{-}6}$ (19 MJ/kg) and EE-POME$_3$ (24 MJ/kg), which lie below the Tier 1 target value.

Finally, the B*POME$_{1\text{-}6}$ compounds extracted into water were identified and quantified. MM- and MB-POMEs were preferentially extracted into the aqueous layer with BB-POMEs demonstrating low water solubility, as suggested by the computational analysis. For example, MM-POME$_{4\text{-}6}$ accounted for 3 g/L, MB-POME$_{2\text{-}6}$ for 4 g/L, and BB-POME$_{1\text{-}5}$ for only 0.3 g/L. The total water solubility of B*POME$_{1\text{-}6}$ was determined to be 7.3 g/L (Table S10). The measured water solubility is a little more than half of the predicted value (14 g/L) and exceeded the target metric (< 20 g/L). There are still limitations to the modeling methodology to predict fuel properties with new molecular structures, like these MB and BB-terminated POMEs.[47] Water solubility is the metric where B*POME$_{1\text{-}6}$ exhibited the greatest advantage when compared with the parent MM-POME$_{3\text{-}6}$ (258 g/L) and the EE-POME$_3$ (predicted solubility of 39 g/L), demonstrating a 35-fold and 5-fold reduction respectively.

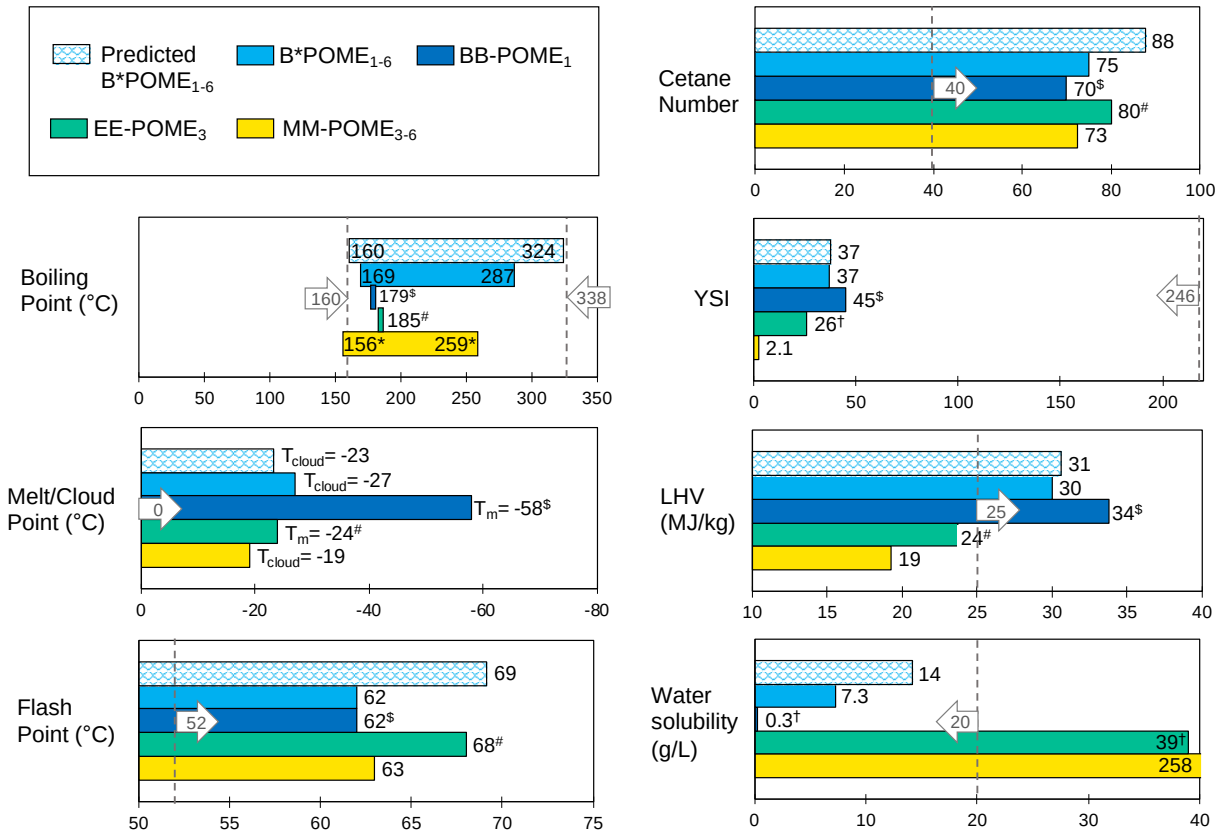

Figure 4. Plots of measured Tier 1 fuel properties for B*POME$_{1\text{-}6}$ compard to predicted fuel properties assuming linear blending, and measured fuel properties for MM-POME$_{3\text{-}6}$, BB-POME$_1$, and EE-POME$_3$. Details of linear blending analysis are in Table S11. The targeted region for each fuel property is indicated by the arrow marked with the specific numerical criterion for diesel blendstocks. *Measured value from Härtl, et al.[21] $Measured value from Fioroni, et al.[24] except for predicted YSI for BB-POME$_1$ #Measured value from Lautenschütz, et al.[19] †Predicted value from Bartholet, et al.[27]

Conclusions

A fuel-property-first approach utilized a computational assessment to identify butyl-terminated POMEs as promising bio-derived diesel blendstocks, especially considering their greater LHV and lower water solubility compared to that of more widely-studied and commercially-available

methyl-terminated POMEs. An acid-catalyzed trans-acetalization reaction was developed to access these targeted species through exchange of the methyl end-groups of the parent MM-POME$_{3-6}$ with butyl end-groups using BuOH. The reaction utilized an Amberlyst-46 acid catalyst at mild reaction conditions (60 °C and atmospheric pressure) to produce the butyl-exchanged POMEs (B*POME$_{1-6}$), enabling scale-up to prepare 100 mL of a product in the desired diesel boiling range for experimental fuel property measurement. Although the present reaction pathway produced a portion of light by-products, they were easily separated and could be potentially recycled. The chemistry reported here represents an alternative to previous reports that utilized formaldehyde as a reagent, and the relative efficiency, sustainability, and economics of these pathways will be an interesting topic of continued investigation.

The measured fuel properties compared well against their predicted values, assuming a linear blending of the individual components, and demonstrated the advantage of the B*POME$_{1-6}$ product over the parent MM-POME$_{3-6}$ and EE-POME$_3$, especially in terms of increased LHV and greatly reduced water solubility. The end-group exchange chemistry is compatible with other potentially renewably-sourced alcohols and mixtures thereof, enabling further exploration of exchanged-POME structures to tune fuel properties for diesel blendstocks.

B*POME$_{1-6}$ compared favorably against the initial Tier 1 screening criteria for CI diesel fuels, specifically where other MM- and EE-terminated POMEs failed. The encouraging results set the foundation to measure Tier 2 criteria, which assess how well these fuel properties blend with a conventional diesel fuel. Tier 2 metrics focus on additional properties including blend cetane number, lubricity, conductivity, oxidation stability, viscosity and compatibility with elastomers

and plastics in the fuel infrastructure, where MM-terminated POMEs have demonstrated shortcomings.[48] Finally, the results reported here also motivate an investigation into the techno-economic and life-cyle analysis of the B*POME$_{1-6}$ conversion pathway in order to identify risks, cost drivers and potential greenhouse gas emissions reductions associated with scale-up and deployment of this product.

Supporting Information

The Supporting Information is available free of charge on the ACS Publications website:

Experimental details; Computed fuel properties; Table of product composition as a function of time during the trans-acetalization reaction; Data for analysis of standard error; Calculated equilibrium product distributions; Results from control experiments without catalyst and without butanol; Calculated thermodynamic equilibrium constants; Table of product compositions with varying BuOH:MM-POME$_{3-6}$ mol ratio; Butyl-exchanged product composition before and after separation; simulated distillation results; Table of water solubility results; Table of predicted fuel properties using a linear blending model.

Acknowledgements

This work was authored in part by the National Renewable Energy Laboratory, operated by Alliance for Sustainable Energy, LLC, for the U.S. Department of Energy (DOE) under Contract No. DE-AC36-08GO28308. This research was conducted as part of the Co-Optimization of Fuels & Engines (Co-Optima) project sponsored by the U.S. Department of Energy – Office of Energy Efficiency and Renewable Energy, Bioenergy Technologies and Vehicle Technologies Offices. Co-Optima is a collaborative project of several national laboratories initiated to simultaneously

accelerate the introduction of affordable, scalable, and sustainable biofuels and high-efficiency, low-emission vehicle engines. Part of this material is based upon work supported by the U.S. Department of Energy's Office of Energy Efficiency and Renewable Energy (EERE) under the Bioenergy Technologies Office (BETO) Program Award Number DE-EE0008726. The views expressed in this article do not necessarily represent the views of the DOE or the U.S. Government. The U.S. Government retains and the publisher, by accepting the article for publication, acknowledges that the U.S. Government retains a nonexclusive, paid-up, irrevocable, worldwide license to publish or reproduce the published form of this work, or allow others to do so, for U.S. Government purposes. The authors thank Trenton J. Wilke for his initial contribution to the development of the end-group exchange reaction.

Corresponding Authors

*Thomas D. Foust. Email: Thomas.Foust@nrel.gov,

*Daniel A. Ruddy. Email: Dan.Ruddy@nrel.gov

Table of Contents Image

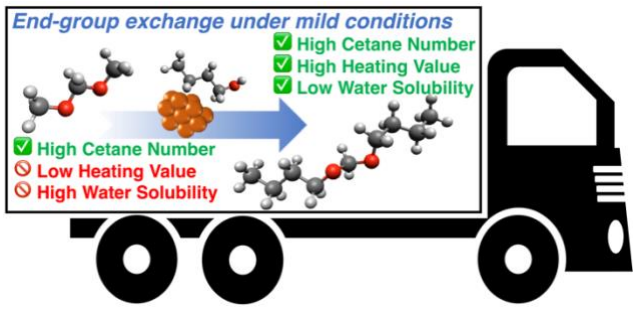

Synopsis

End-group exchange chemistry employing renewable butanol improves two key diesel fuel properties for high-cetane polyoxymethylene ethers.

Author Contributions

The manuscript was written through contributions of all authors. All authors have given approval to the final version of the manuscript.

References

(1) U.S. Energy Information Administration. *Annual Energy Outlook 2020 with Projections to 2050*; 2020.

(2) IEA. *Global Energy & CO_2 Status Report 2019*; Paris, 2019.

(3) Awad, O. I.; Ma, X.; Kamil, M.; Ali, O. M.; Ma, Y.; Shuai, S. Overview of Polyoxymethylene Dimethyl Ether Additive as an Eco-Friendly Fuel for an Internal Combustion Engine: Current Application and Environmental Impacts. *Sci. Total Environ.* **2020**, *715*, 136849. https://doi.org/10.1016/j.scitotenv.2020.136849.

(4) Li, B.; Li, Y.; Liu, H.; Liu, F.; Wang, Z.; Wang, J. Combustion and Emission Characteristics of Diesel Engine Fueled with Biodiesel/PODE Blends. *Appl. Energy* **2017**, *206* (September), 425–431. https://doi.org/10.1016/j.apenergy.2017.08.206.

(5) Liu, H.; Wang, Z.; Zhang, J.; Wang, J.; Shuai, S. Study on Combustion and Emission Characteristics of Polyoxymethylene Dimethyl Ethers/Diesel Blends in Light-Duty and Heavy-Duty Diesel Engines. *Appl. Energy* **2017**, *185*, 1393–1402. https://doi.org/10.1016/j.apenergy.2015.10.183.

(6) Burger, J.; Ströfer, E.; Hasse, H. Chemical Equilibrium and Reaction Kinetics of the Heterogeneously Catalyzed Formation of Poly(Oxymethylene) Dimethyl Ethers from Methylal and Trioxane. *Ind. Eng. Chem. Res.* **2012**, *51* (39), 12751–12761. https://doi.org/10.1021/ie301490q.

(7) Burger, J.; Siegert, M.; Ströfer, E.; Hasse, H. Poly(Oxymethylene) Dimethyl Ethers as Components of Tailored Diesel Fuel: Properties, Synthesis and Purification Concepts. *Fuel* **2010**, *89* (11), 3315–3319. https://doi.org/10.1016/j.fuel.2010.05.014.

(8) Held, M.; Tönges, Y.; Pélerin, D.; Härtl, M.; Wachtmeister, G.; Burger, J. On the Energetic Efficiency of Producing Polyoxymethylene Dimethyl Ethers from CO2 Using Electrical Energy. *Energy Environ. Sci.* **2019**, *12* (3), 1019–1034. https://doi.org/10.1039/c8ee02849d.

(9) Feng, W.; Ji, P.; Chen, B.; Zheng, D. Analysis of Methanol Production from Biomass Gasification. *Chem. Eng. Technol.* **2011**, *34* (2), 307–317. https://doi.org/10.1002/ceat.201000346.

(10) Holmgren, K. M.; Andersson, E.; Berntsson, T.; Rydberg, T. Gasification-Based Methanol Production from Biomass in Industrial Clusters: Characterisation of Energy Balances and Greenhouse Gas Emissions. *Energy* **2014**, *69*, 622–637. https://doi.org/10.1016/j.energy.2014.03.058.

(11) Morandin, M.; Harvey, S. *Methanol via Biomass Gasification Thermodynamic Performances and Process Integration Aspects in Swedish Chemical Cluster and Pulp and Paper Sites*; Göteborg, Sweden, 2015. https://doi.org/10.13140/RG.2.1.4272.1443.

(12) White, J. L. Methanol-to-Hydrocarbon Chemistry: The Carbon Pool (r)Evolution. *Catal. Sci. Technol.* **2011**, *1* (9), 1630–1635. https://doi.org/10.1039/c1cy00197c.

(13) Stöcker, M. Methanol-to-Hydrocarbons: Catalytic Materials and Their Behavior. *Microporous Mesoporous Mater.* **1999**, *29* (1–2), 3–48. https://doi.org/10.1016/S1387-1811(98)00319-9.

(14) Keil, F. J. Methanol-to-Hydrocarbons: Process Technology. *Microporous Mesoporous Mater.* **1999**, *29* (1–2), 49–66. https://doi.org/10.1016/S1387-1811(98)00320-5.

(15) Grim, R. G.; To, A. T.; Farberow, C. A.; Hensley, J. E.; Ruddy, D. A.; Schaidle, J. A. Growing the Bioeconomy through Catalysis: A Review of Recent Advancements in the Production of Fuels and Chemicals from Syngas-Derived Oxygenates. *ACS Catal.* **2019**, *9* (5), 4145–4172. https://doi.org/10.1021/acscatal.8b03945.

(16) To, A. T.; Wilke, T. J.; Nelson, E.; Nash, C. P.; Bartling, A.; Wegener, E. C.; Unocic, K. A.; Habas, S. E.; Foust, T. D.; Ruddy, D. A. Dehydrogenative Coupling of Methanol for the Gas-Phase, One-Step Synthesis of Dimethoxymethane over Supported Copper Catalysts. *ACS Sustain. Chem. Eng.* **2020**, *8* (32), 12151–12160. https://doi.org/10.1021/acssuschemeng.0c03606.

(17) Ruijun, Z.; Xibin, W.; Haiyan, M.; Zuohua, H.; Jing, G.; Deming, J. Performance and Emission Characteristics of Diesel Engines Fueled with Diesel-Dimethoxymethane (DMM) Blends. *Energy and Fuels* **2009**, *23* (1), 286–293. https://doi.org/10.1021/ef8005228.

(18) Kang, M. R.; Song, H. Y.; Jin, F. X.; Chen, J. Synthesis and Physicochemical Characterization of Polyoxymethylene Dimethyl Ethers. *J. Fuel Chem. Technol.* **2017**, *45* (7), 837–845. https://doi.org/10.1016/s1872-5813(17)30040-3.

(19) Lautenschütz, L.; Oestreich, D.; Seidenspinner, P.; Arnold, U.; Dinjus, E.; Sauer, J. Physico-Chemical Properties and Fuel Characteristics of Oxymethylene Dialkyl Ethers.

Fuel **2016**, *173*, 129–137. https://doi.org/10.1016/j.fuel.2016.01.060.

(20) Omari, A.; Heuser, B.; Pischinger, S.; Rüdinger, C. Potential of Long-Chain Oxymethylene Ether and Oxymethylene Ether-Diesel Blends for Ultra-Low Emission Engines. *Appl. Energy* **2019**, *239* (February), 1242–1249. https://doi.org/10.1016/j.apenergy.2019.02.035.

(21) Härtl, M.; Gaukel, K.; Pélerin, D.; Wachtmeister, G. Oxymethylene Ether as Potentially CO2-Neutral Fuel for Clean Diesel Engines Part 1: Engine Testing. *MTZ Worldw.* **2017**, *78* (2), 52–59. https://doi.org/10.1007/s38313-016-0163-6.

(22) Baranowski, C. J.; Bahmanpour, A. M.; Kröcher, O. Catalytic Synthesis of Polyoxymethylene Dimethyl Ethers (OME): A Review. *Appl. Catal. B Environ.* **2017**, *217*, 407–420. https://doi.org/10.1016/j.apcatb.2017.06.007.

(23) ASTM International. *D975-20a Standard Specification for Diesel Fuel*; West Conshohocken, PA, 2020. https://doi.org/https://doi.org/10.1520/D0975-20A.

(24) Fioroni, G.; Fouts, L.; Luecke, J.; Vardon, D.; Huq, N.; Christensen, E.; Huo, X.; Alleman, T.; McCormick, R.; Kass, M.; Polikarpov, E.; Kukkadapu, G.; Whitesides, R. A. Screening of Potential Biomass-Derived Streams as Fuel Blendstocks for Mixing Controlled Compression Ignition Combustion. *SAE Int. J. Adv. Curr. Pr. Mobil.* **2019**, *1* (3), 1117–1138. https://doi.org/10.4271/2019-01-0570.

(25) McCormick, R. L.; Fioroni, G.; Fouts, L.; Christensen, E.; Yanowitz, J.; Polikarpov, E.; Albrecht, K.; Gaspar, D. J.; Gladden, J.; George, A. Selection Criteria and Screening of Potential Biomass-Derived Streams as Fuel Blendstocks for Advanced Spark-Ignition Engines. *SAE Int. J. Fuels Lubr.* **2017**, *10* (2), 442–460. https://doi.org/10.4271/2017-01-0868.

(26) Montgomery, M. J.; Das, D. D.; McEnally, C. S.; Pfefferle, L. D. Analyzing the Robustness of the Yield Sooting Index as a Measure of Sooting Tendency. *Proc. Combust. Inst.* **2019**, *37* (1), 911–918. https://doi.org/10.1016/j.proci.2018.06.105.

(27) Bartholet, D.; Arellano-Treviño, M. A.; Chan, F. L.; Lucas, S.; Zhu, J.; St.John, P.; Fioroni, G.; Hays, C.; Alleman, T. L.; McEnally, C. S.; Pfefferle, L. D.; Ruddy, D. A.; Windom, B.; Foust, T. D.; Reardon, K. F. Property Predictions of Structurally Diverse Polyoxymethylene Ethers as Potential Diesel Blendstocks. *Fuel*, **2021**, *295*, 120509. https://doi.org/10.1016/j.fuel.2021.120509

(28) Geng, P.; Furey, R.; Konzack, A. Calculation of Heating Value for Gasoline Containing Ethanol. *SAE Int. J. Fuels Lubr.* **2010**, *3* (2), 2010-01–1517. https://doi.org/10.4271/2010-01-1517.

(29) Huq, N. A.; Huo, X.; Hafenstine, G. R.; Tifft, S. M.; Stunkel, J.; Christensen, E. D.; Fioroni, G. M.; Fouts, L.; McCormick, R. L.; Cherry, P. A.; McEnally, C. S.; Pfefferle, L. D.; Wiatrowski, M. R.; Benavides, P. T.; Biddy, M. J.; Connatser, R. M.; Kass, M. D.; Alleman, T. L.; St John, P. C.; Kim, S.; Vardon, D. R. Performance-Advantaged Ether Diesel Bioblendstock Production by a Priori Design. *Proc. Natl. Acad. Sci. U. S. A.* **2019**, *116* (52), 26421–26430. https://doi.org/10.1073/pnas.1911107116.

(30) Huo, X.; Huq, N. A.; Stunkel, J.; Cleveland, N. S.; Starace, A. K.; Settle, A. E.; York, A. M.; Nelson, R. S.; Brandner, D. G.; Fouts, L.; St. John, P. C.; Christensen, E. D.; Luecke, J.; Mack, J. H.; McEnally, C. S.; Cherry, P. A.; Pfefferle, L. D.; Strathmann, T. J.; Salvachúa, D.; Kim, S.; McCormick, R. L.; Beckham, G. T.; Vardon, D. R. Tailoring Diesel Bioblendstock from Integrated Catalytic Upgrading of Carboxylic Acids: A "Fuel Property First" Approach. *Green Chem.* **2019**, *21* (21), 5813–5827.

https://doi.org/10.1039/c9gc01820d.

(31) Hafenstine, G. R.; Huq, N. A.; Conklin, D. R.; Wiatrowski, M. R.; Huo, X.; Guo, Q.; Unocic, K. A.; Vardon, D. R. Single-Phase Catalysis for Reductive Etherification of Diesel Bioblendstocks. *Green Chem.* **2020**, *22* (Scheme 1). https://doi.org/10.1039/d0gc00939c.

(32) Khan, I.; Akhtar, M. W. Bioenergy Production From Plant Biomass: Bioethanol From Concept To Reality. *Nat. Preced.* **2011**. https://doi.org/10.1038/npre.2011.6286.1.

(33) Ezeji, T. C.; Qureshi, N.; Blaschek, H. P. Bioproduction of Butanol from Biomass: From Genes to Bioreactors. *Curr. Opin. Biotechnol.* **2007**, *18* (3), 220–227. https://doi.org/10.1016/j.copbio.2007.04.002.

(34) Haltenort, P.; Lautenschütz, L.; Arnold, U.; Sauer, J. (Trans)Acetalization Reactions for the Synthesis of Oligomeric Oxymethylene Dialkyl Ethers Catalyzed by Zeolite BEA25. *Top. Catal.* **2019**, *62* (5–6), 551–559. https://doi.org/10.1007/s11244-019-01188-9.

(35) Ramírez, E.; Bringué, R.; Fité, C.; Iborra, M.; Tejero, J.; Cunill, F. Role of Ion-Exchange Resins as Catalyst in the Reaction-Network of Transformation of Biomass into Biofuels. *J. Chem. Technol. Biotechnol.* **2017**, *92* (11), 2775–2786. https://doi.org/10.1002/jctb.5352.

(36) Wu, L.; Moteki, T.; Gokhale, A. A.; Flaherty, D. W.; Toste, F. D. Production of Fuels and Chemicals from Biomass: Condensation Reactions and Beyond. *Chem* **2016**, *1* (1), 32–58. https://doi.org/10.1016/j.chempr.2016.05.002.

(37) Badia, J. H.; Fité, C.; Bringué, R.; Iborra, M.; Cunill, F. Catalytic Activity and Accessibility of Acidic Ion-Exchange Resins in Liquid Phase Etherification Reactions. *Top. Catal.* **2015**, *58* (14), 919–932. https://doi.org/10.1007/s11244-015-0460-3.

(38) Pérez, M. A.; Bringué, R.; Iborra, M.; Tejero, J.; Cunill, F. Ion Exchange Resins as Catalysts for the Liquid-Phase Dehydration of 1-Butanol to Di-n-Butyl Ether. *Appl. Catal. A Gen.* **2014**, *482*, 38–48. https://doi.org/10.1016/j.apcata.2014.05.017.

(39) Schmitz, N.; Homberg, F.; Berje, J.; Burger, J.; Hasse, H. Chemical Equilibrium of the Synthesis of Poly(Oxymethylene) Dimethyl Ethers from Formaldehyde and Methanol in Aqueous Solutions. *Ind. Eng. Chem. Res.* **2015**, 54 (25), 6409–6417. https://doi.org/10.1021/acs.iecr.5b01148.

(40) Peschla, R.; Garćía, B. C.; Albert, M.; Kreiter, C.; Maurer, G. Chemical Equilibrium and Liquid-Liquid Equilibrium in Aqueous Solutions of Formaldehyde and 1-Butanol. *Ind. Eng. Chem. Res.* **2003**, 42 (7), 1508–1516. https://doi.org/10.1021/ie020743o.

(41) Hahnenstein, I.; Hasse, H.; ZKreiter, C. G.; Maurer, G. ^{1}H- and ^{13}C-NMR Spectroscopic Study of Chemical Equilibria in Solutions of Formaldehyde in Water, Deuterium Oxide, and Methanol. *Ind. Eng. Chem. Res.* **1994**, *33 (4)*, 1022-1029. https://doi.org/10.1021/ie00028a033

(42) Maiwald, M.; Fischer, H. H.; Ott, M.; Peschla, R.; Kuhnert C.; Kreiter, C. G.; Maurer, G.; Hasse, H. Quantitative NMR Spectroscopy of Complex Liquid Mixtures: Methods and Results for Chemical Equilibria in Formaldehyde-Water-Methanol at Temperatures up to 383 K. *Ind. Eng. Chem. Res.* **2003**, *42 (2)*, 259-266. https://doi.org/10.1021/ie0203072

(43) Hughes, L. D.; Palmer, D. S.; Nigsch, F.; Mitchell, J. B. O. Why Are Some Properties More Difficult to Predict than Others? A Study of QSPR Models of Solubility, Melting Point, and Log P. *J. Chem. Inf. Model.* **2008**, *48* (1), 220–232. https://doi.org/10.1021/ci700307p.

(44) McEnally, C. S.; Xuan, Y.; St John, P. C.; Das, D. D.; Jain, A.; Kim, S.; Kwan, T. A.;

Tan, L. K.; Zhu, J.; Pfefferle, L. D. Sooting Tendencies of Co-Optima Test Gasolines and Their Surrogates. *Proc. Combust. Inst.* **2019**, *37* (1), 961–968. https://doi.org/10.1016/j.proci.2018.05.071.

(45) Kessler, T.; Sacia, E. R.; Bell, A. T.; Mack, J. H. Artificial Neural Network Based Predictions of Cetane Number for Furanic Biofuel Additives. *Fuel* **2017**, *206*, 171–179. https://doi.org/10.1016/j.fuel.2017.06.015.

(46) St.John, P. C.; Kairys, P.; Das, D. D.; McEnally, C. S.; Pfefferle, L. D.; Robichaud, D. J.; Nimlos, M. R.; Zigler, B. T.; McCormick, R. L.; Foust, T. D.; Bomble, Y. J.; Kim, S. A Quantitative Model for the Prediction of Sooting Tendency from Molecular Structure. *Energy and Fuels* **2017**, *31* (9), 9983–9990. https://doi.org/10.1021/acs.energyfuels.7b00616.

(47) Hewitt, M.; Cronin, M. T. D.; Enoch, S. J.; Madden, J. C.; Roberts, D. W.; Dearden, J. C. In Silico Prediction of Aqueous Solubility: The Solubility Challenge. *J. Chem. Inf. Model.* **2009**, *49* (11), 2572–2587. https://doi.org/10.1021/ci900286s.

(48) Kass, M.; Wissink, M.; Janke, C.; Connatser, R.; Curran, S. Compatibility of Elastomers with Polyoxymethylene Dimethyl Ethers and Blends with Diesel. *SAE Tech. Pap.* **2020**, *2020-01–06*, 1–11. https://doi.org/10.4271/2020-01-0620.